A CZS-decorated Al-MOF S-scheme heterojunction for concurrently photocatalytic generating H_2 and Methylene Blue degradation under visible-light

Zhou Shujun [a], Zhang Tianyuan [a], Wang Liping [a], Wang Zhijuan [a*], Chen Hongjin [a], Miao Yingchun [a*]

[a] Yunnan Key Laboratory of Crystalline Porous Organic Functional Materials, College of Chemistry and Material Engineering, Qujing Normal University, Qujing 655011, PR China.

Text S1

The reagents used in the experiments concluded aluminum nitrate nonahydrate ($Al(NO_3)_3·9H_2O$, 99.0%, Fucheng of Tianjin), 2-aminoterephthalic acid (NH_2-BDC, 98%, Damas-Beta), N,N-dimethyl formamide (DMF, 99.5%, Xilong Scientific), anhydrous ethanol (99.7%, Xilong Scientific), ethylene glycol (EG, 99.5%, Xilong Scientific), cadmium acetate dihydrate ($Cd(Ac)_2·2H_2O$, 98%, Damas-Beta), zinc acetate dihydrate ($Zn(Ac)_2·2H_2O$, 99.0%, General-Reagent), thiourea (99.5%, General-Reagent), triethanolamine (TEOA, 98%, Macklin), eosin-Y (EY, 85%, Yuanye), methanol (99.5%, Xilong Scientific) , triethylamine (TEA, 99.0%, Fengchuan of Tianjin), ascorbic acid (99.7%, Xilong Scientific), sodium sulfide (Na_2S, 99%, Damas-Beta), sodium sulphite (Na_2SO_3, 98%, Aladdin), L-lactic acid (90%, Macklin), methylene blue (MB, 98.5%, Kelong of Chengdu), ethylenediaminetetraacetic acid disodium (EDTA-2Na, 97.0%, Sigma-Aldrich), 1,4-benzoquinone (p-BQ, 98.0%, Meryer of Shanghai), 2-furfuryl alcohol (FFA, 98%, Aladdin) and tert-butyl alcohol (TBA, 99.7%, Sigma-Aldrich). All the reagents were used directly without any pretreatment.

* Corresponding Author.
Email-address: boying2004@163.com (Wang Zhijuan), miaoyingchun1979@126.com (Miao Yingchun).

Text S2

The morphologies, microstructures and surface elemental composition were detected through SEM (S4800, Hitachi) equipped with an energy-dispersive X-ray spectrometer (EDS) and transmission electron microscopy (TEM, JEM-2100Plus, Japan). The phase compositions of Al-MOF and Al-MOF/x-CZS were explored by X-ray diffraction (XRD, D8 ADVANCE, Bruker, Germany). Functional groups of the as-prepared photocatalysts were identified via Fourier-transform infrared spectra (FTIR, PerkinElmer, American). The specific surface areas and pore structures were calculated from N_2 adsorption-desorption isotherms tested via a surface-area pore analyzer (tristar II3020, American). The surface elemental valence state and valence band spectra were measured by X-ray photoelectron spectroscopy (XPS, ESCALab 250Xi, Thermo Fisher). The ultraviolet-visible diffuse reflectance spectra (DRS) were derived from a TU-1901 spectrophotometer. Photoluminescence emission spectra (PL) were observed using a Fluorescence spectrometer (F4600, HITACHI, Japan) at the excitation wavelength of 375 nm. Time-resolved PL decay curves (TRPL) were detected via a fluorescence spectrometer (FLS980, Edinburg, England). An electrochemical workstation (CH1760D, China) with a three-electrode electrochemical system was applied to conduct the tests of chemical impedance spectroscopy (EIS), Mott-Schottky (MS) and transient photocurrent responses (i-t). Samples were adhered to an ITO glass electrode or a glassy carbon electrode, which was then served as the working electrode. Saturated calomel electrode and platinum sheet electrode were used as reference electrode and counter electrode, respectively. The concentration of electrolyte (Na_2SO_4 solution) was 0.5 mol L^{-1}.

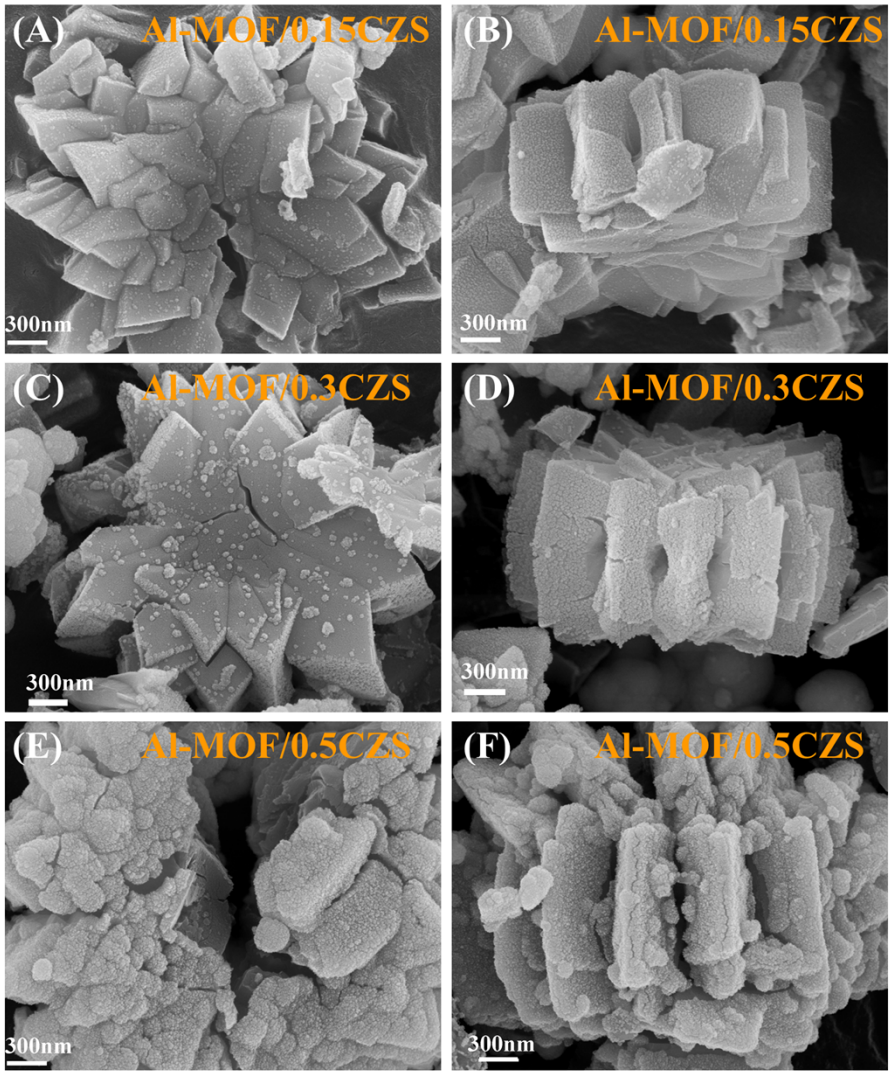

Fig S1. SEM images of (A-B) Al-MOF/0.15CZS, (C-D) Al-MOF/0.3CZS and (E-F) Al-MOF/0.5CZS.

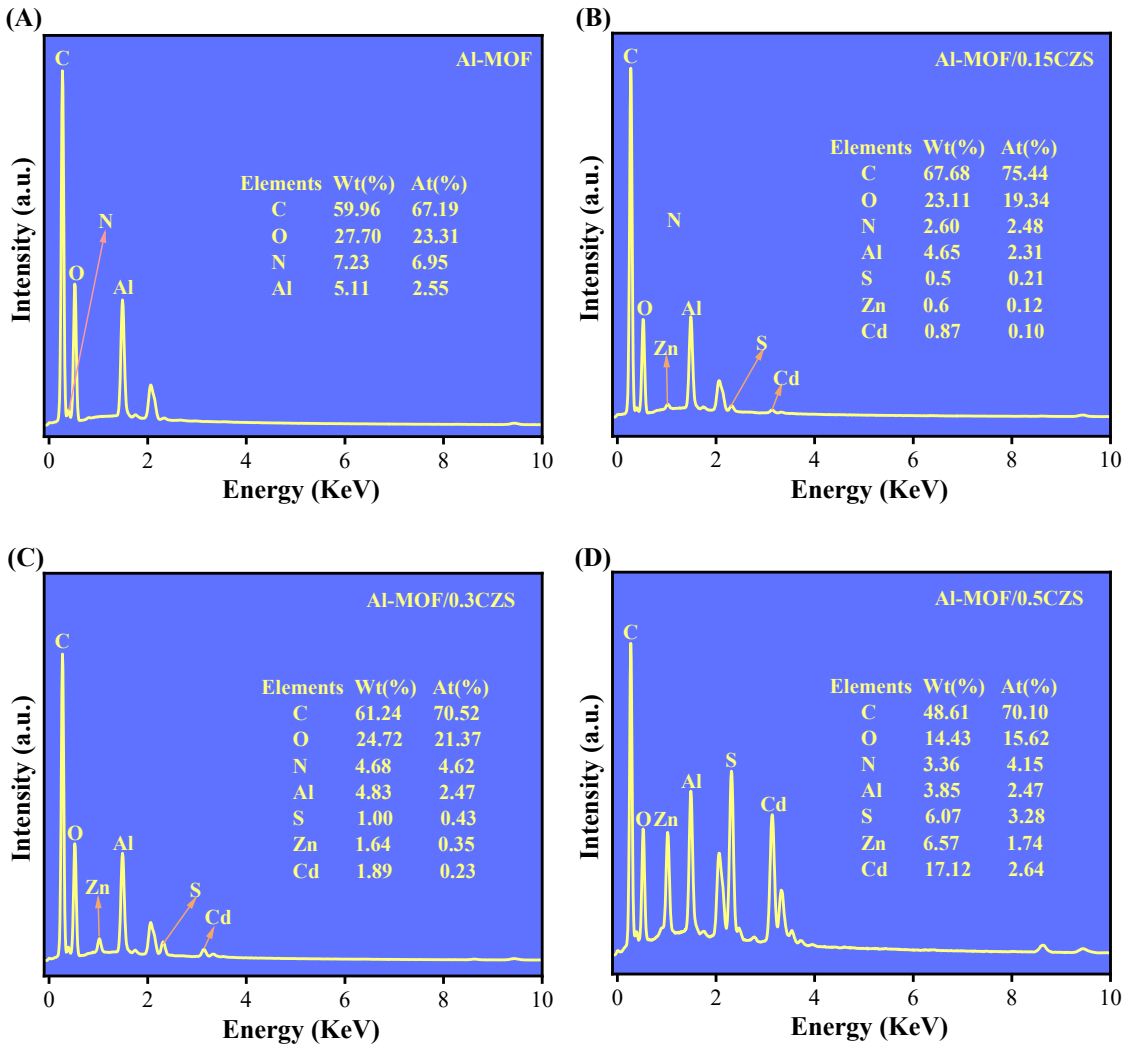

Fig S2. EDS spectra of (A) Al-MOF, (B) Al-MOF/0.15CZS, (C) Al-MOF/0.3CZS and (D) Al-MOF/0.5CZS.

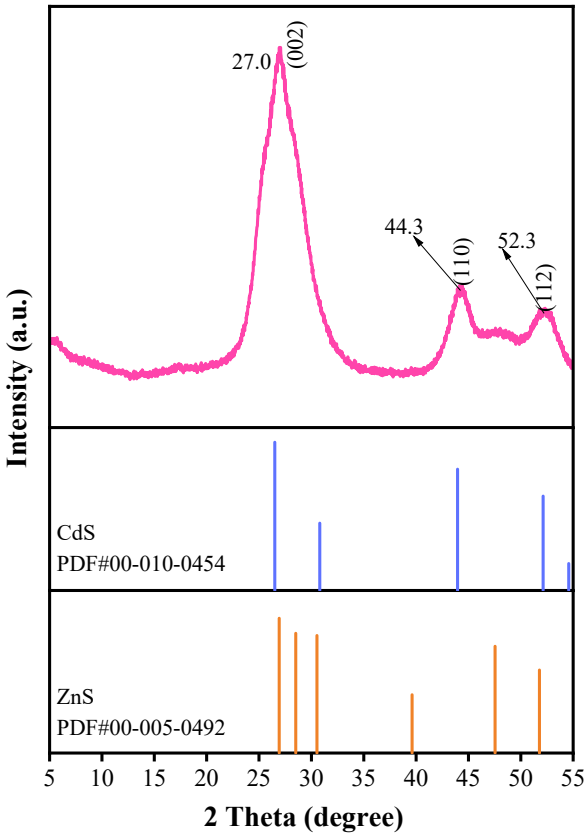

Fig S3. XRD pattern of CZS.

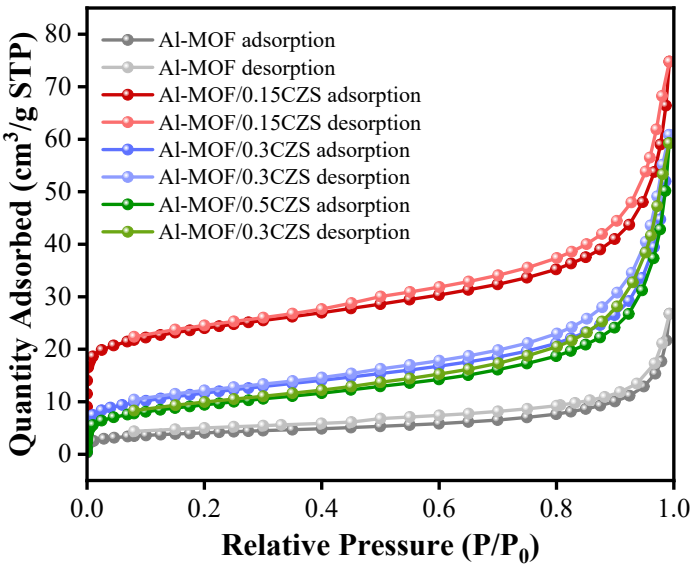

Fig S4. N_2 adsorption-desorption isotherms of photocatalysts.

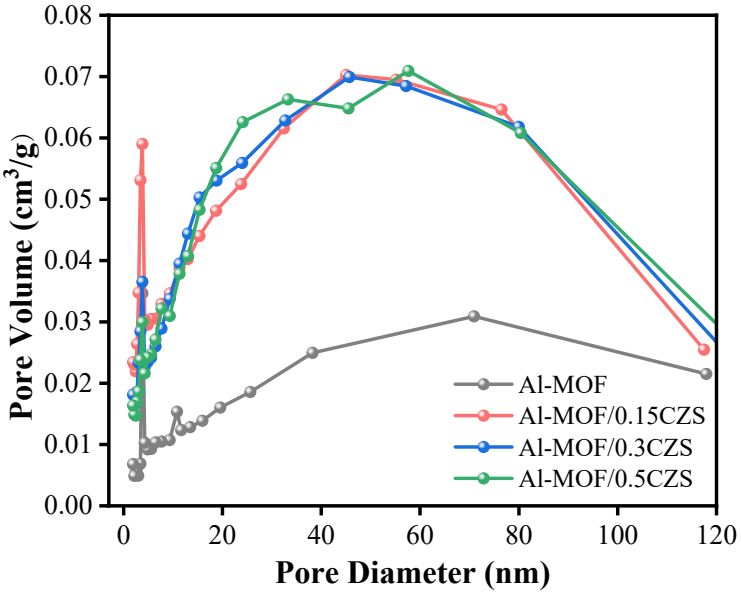

Fig S5. Pore diameter distribution of photocatalysts.

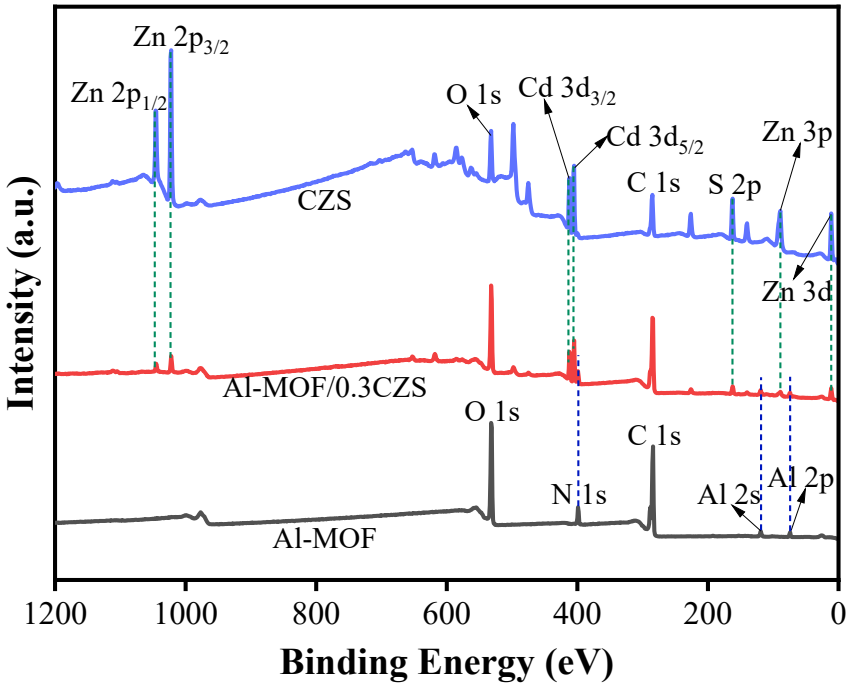

Fig S6. XPS spectra of Al-MOF, CZS and Al-MOF/0.3CZS.

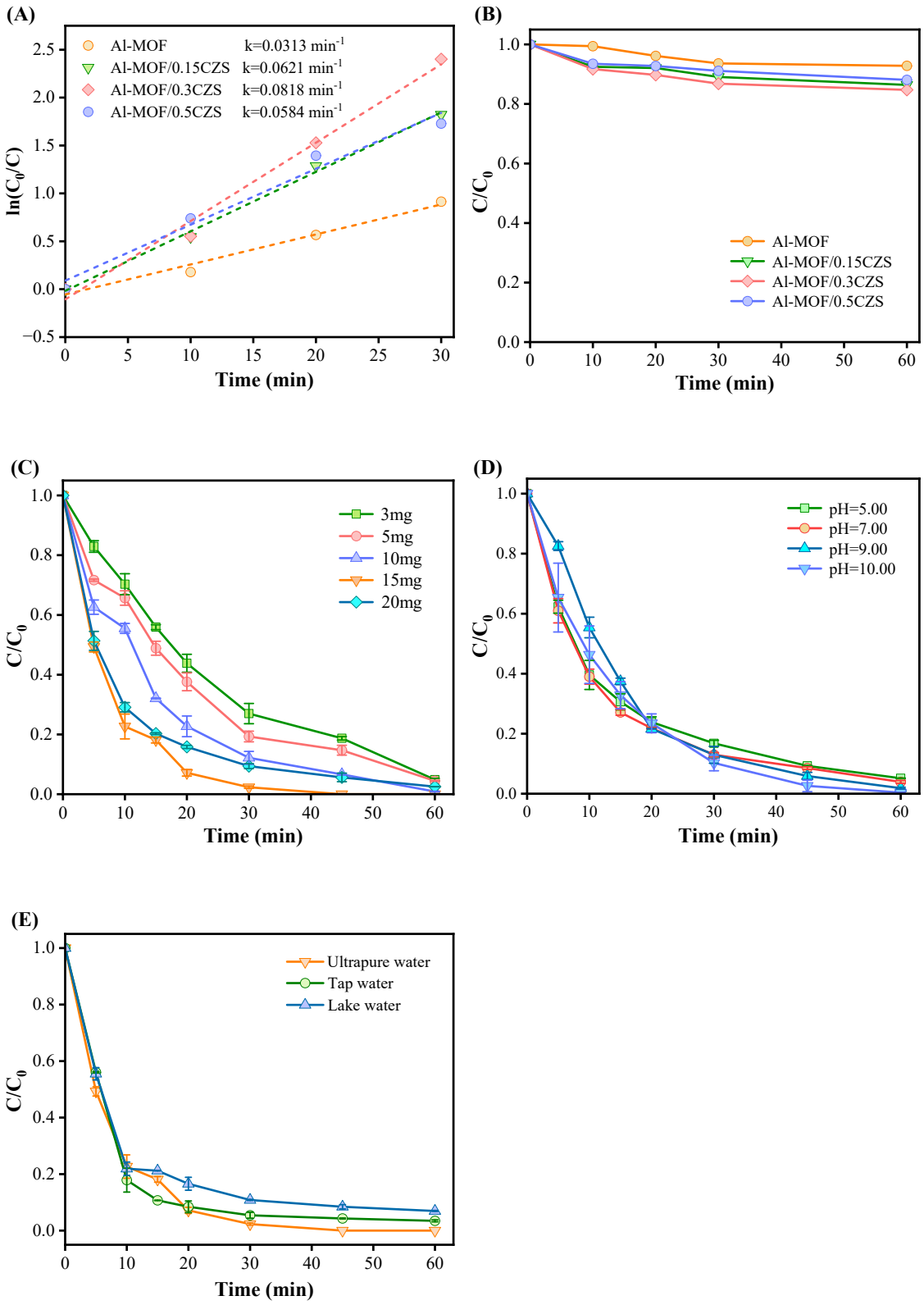

Fig S7. (A) Kinetic fitting curves for MB degradation with various photocatalysts, (B) the adsorption of MB on different photocatalysts in the dark, the influences of (C) Al-MOF/0.3CZS dosage, (D) initial solution pH and (E) various water environments on the MB degradation. (experiment conditions: $[MB]_0$=10 mg L^{-1}, the photocatalyst

amount for (A) and (B) was 0.1 g L^{-1} and the Al-MOF/0.3CZS amount for (D) and (E) was 0.15 g L^{-1})

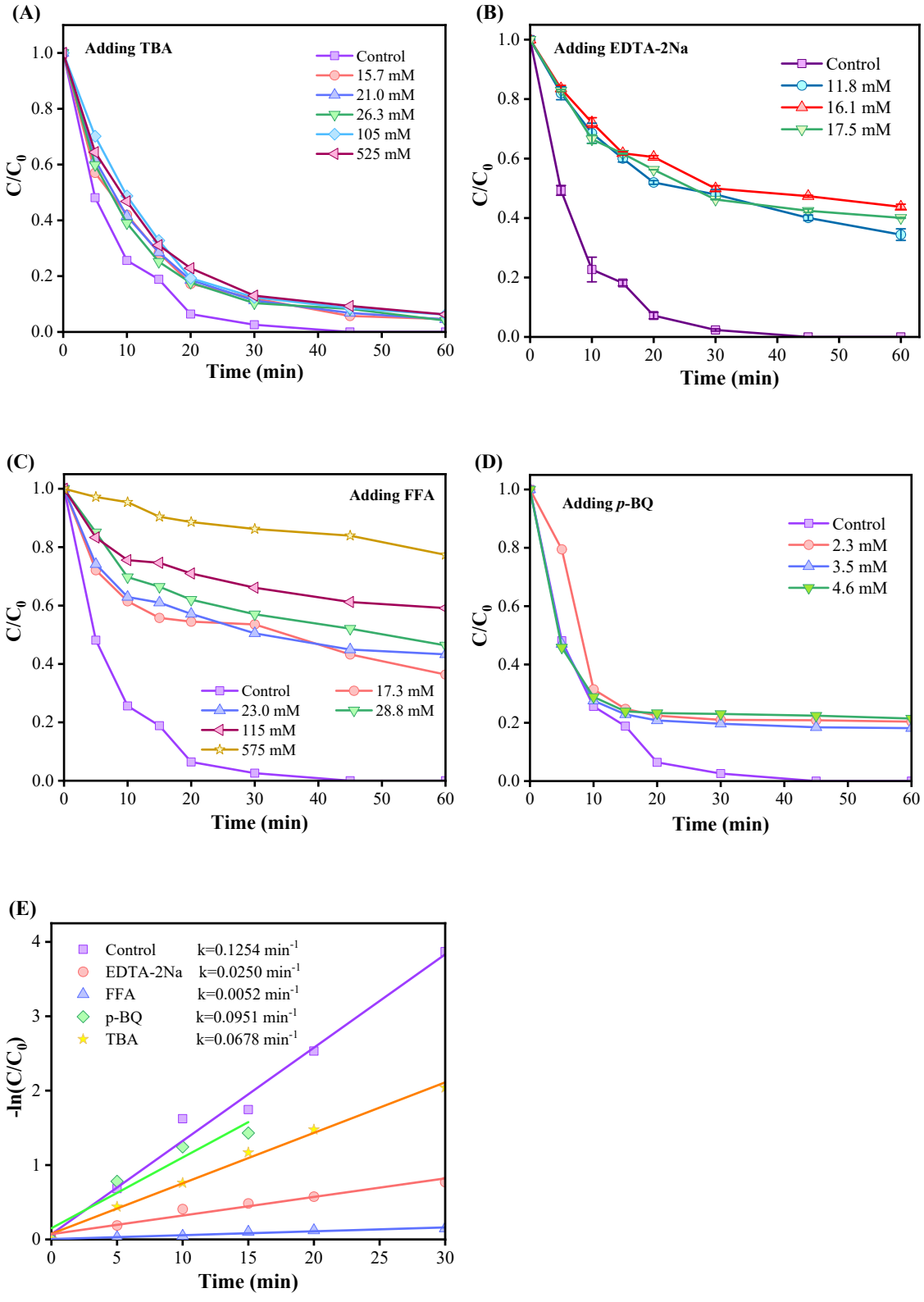

Fig. S8. Influences of (A) TBA, (B) EDTA-2Na, (C) FFA and (D) p-BQ on the MB degradation; (E) Kinetic fitting curves for MB degradation on Al-MOF/0.3CZS when adding trapping agents. (experiment conditions: $[MB]_0$=10 mg L^{-1}, [Al-MOF/0.3CZS]=0.15 g L^{-1})

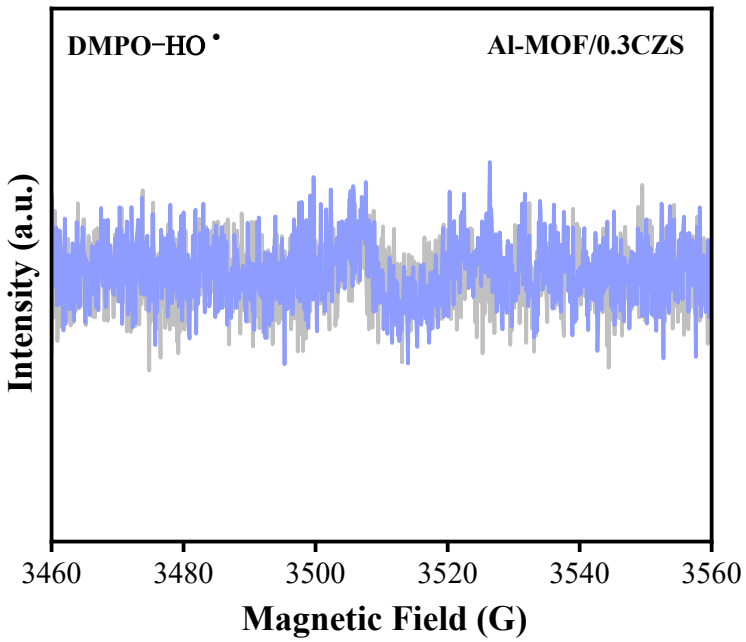

Fig. S9. EPR spectra of DMPO−•OH of Al-MOF/0.3CZS

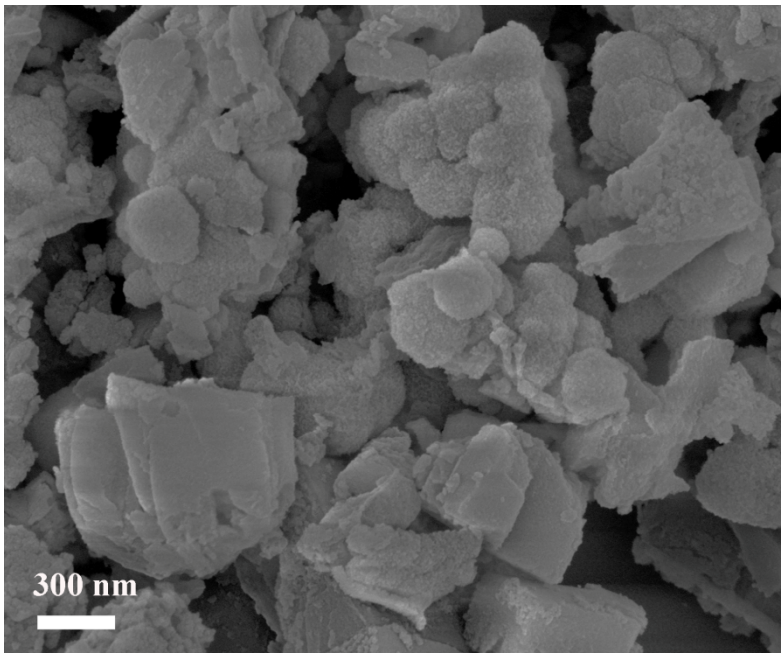

Fig S10. SEM morphology of used Al-MOF/0.3CZS.

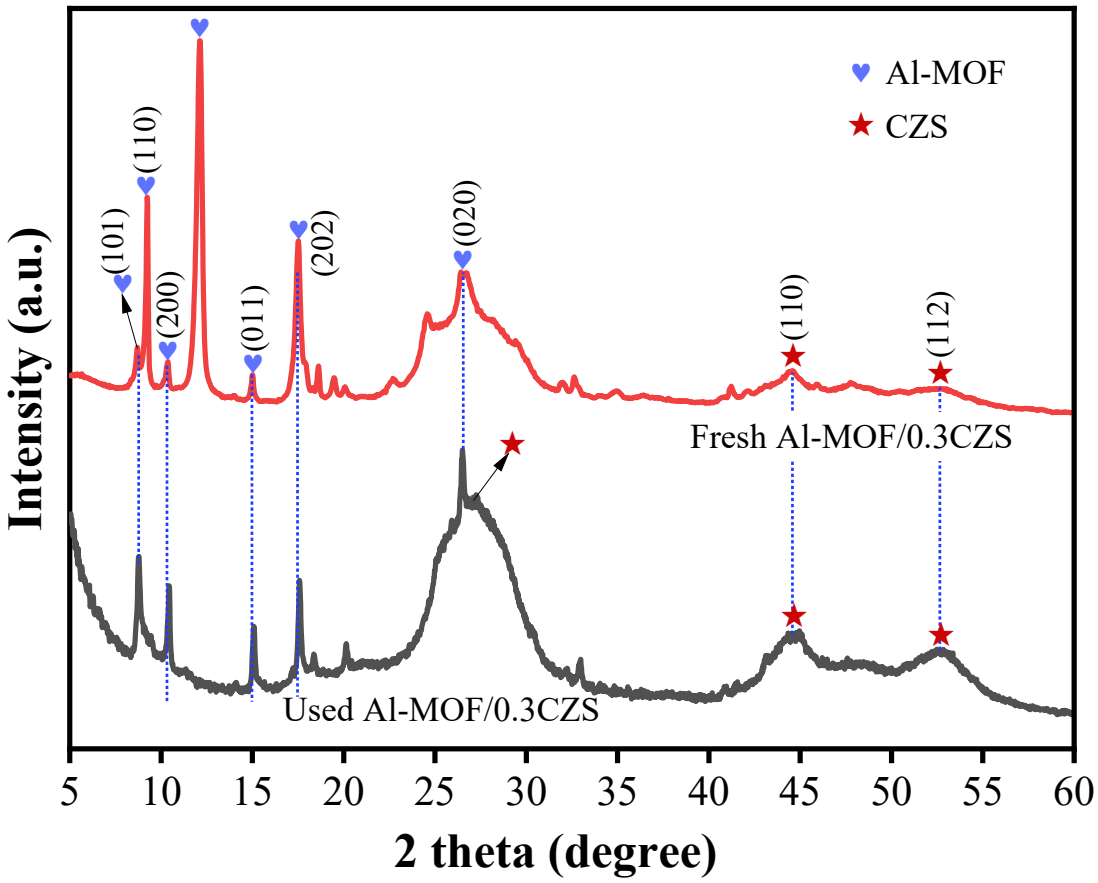

Fig S11. XRD spectra of fresh and used Al-MOF/0.3CZS.

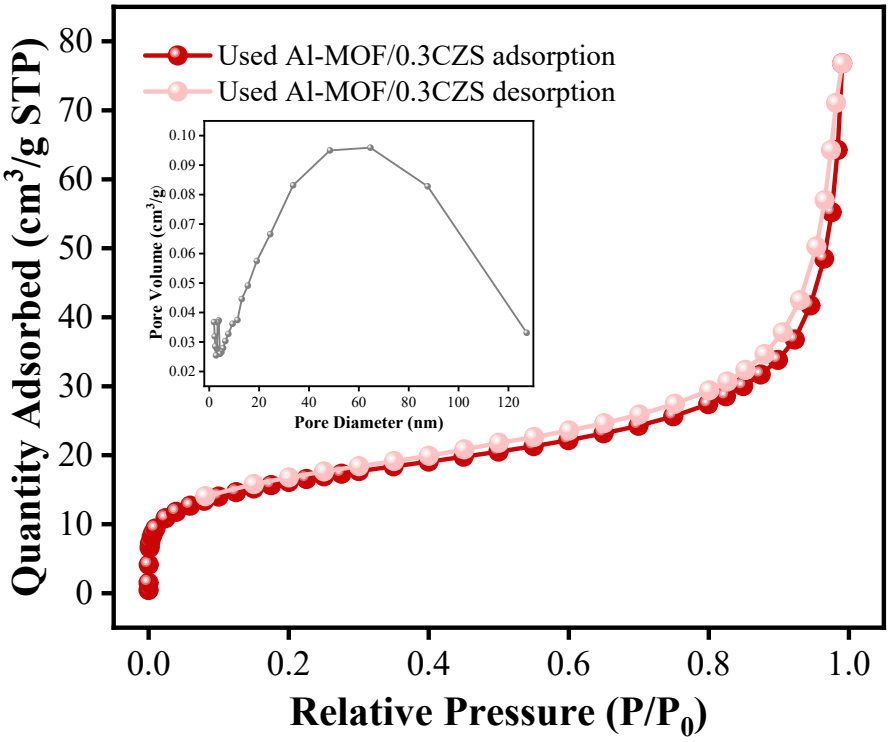

Fig S12. N_2 adsorption-desorption isotherms and pore diameter distribution of used Al-MOF/0.3CZS.

Table S1 The Zn and Cd contents of Al-MOF/x-CZS detected via ICP-MS.

Samples	Theoretical mass percentage of Zn (%)	Measured mass percentage of Zn (%)	Theoretical mass percentage of Cd (%)	Measured mass percentage of Cd (%)	Measured molar ratio of Zn to Cd
Al-MOF/0.15CZS	4.33	4.27	7.44	6.21	1.18
Al-MOF/0.3CZS	7.74	8.61	13.31	15.29	0.97
Al-MOF/0.5CZS	11.32	9.04	19.46	16.02	0.97

Table S2 The pore structures of Al-MOF and Al-MOF/x-CZS.

Samples	Specific surface areas (m^2 g^{-1})	Pore Volume (m^3 g^{-1})	Average pore diameter (nm)
Al-MOF	14.76	0.039	14.6
Al-MOF/0.15CZS	87.61	0.091	10.9
Al-MOF/0.3CZS	41.75	0.086	12.9
Al-MOF/0.5CZS	33.87	0.086	13.7
Used Al-MOF/0.3CZS	58.43	0.107	12.3

Table S3 The metal element contents of Al-MOF/0.3CZS before and after usage detected via ICP-MS.

Samples	Measured mass percentage of Zn (%)	Measured mass percentage of Cd (%)	Measured mass percentage of Al (%)
fresh Al-MOF/0.3CZS	8.61	15.29	7.22
used Al-MOF/0.5CZS	3.51	13.04	7.01

Table S4 Comparison of photocatalytic H_2 production performance with some reported photocatalysts.

Photocatalysts	**Reaction conditions**	**Light source**	**H_2 rate ($\mu mol\ g^{-1}\ h^{-1}$)**	**Reference**
CdS/UiO-67-NH_2	10% TEOA and 0.1 M Na_2SO_3/Na_2S; 20 mg of catalyst	600 W xenon lamp with a filter ($\lambda > 320$ nm)	487.5	1
Co_3O_4/NH_2-MIL-53(Al)	10 mg of catalyst	White light	~1400	2

	and 10 mg of eosin-Y (EY)	5 W		
ZCS@Cu/Fe-MOF	90 mL of deionized water and 10 mL of lactic acid; 0.1 g of catalyst	300 W xenon lamp with a filter (λ > 420 nm)	1563.96	3
Sv-ZIS@NMFe-2	90 mL of deionized water and 10 mL of lactic acid; 20 mg of catalyst	300 W xenon lamp with a filter (λ > 420 nm)	5710	4
Cu-MOF/$ZnIn_2S_4$	100 ml of deionized water containing 20 % triethanolamine (TEOA); 0.2 g of catalyst	300 W xenon lamp	300	5
Co-MOF/H-g-C_3N_4	10 mg of catalyst powder and 20 mg of sensitizer; 30 mL TEOA	—	1033	6
AS@CZS	80 mL of ethanol aqueous solution (24 mL ethanol +56 mL water); 50 mg of catalyst	300 W xenon lamp (560 mW/cm^2)	3023	7
CdS@Ag@ZnS	Ethanol aqueous solution (30 vol%, 80 mL); 50 mg of catalyst	300 W xenon lamp	2810	8

ZnS/TiO_2	50 mL of water including 1.37 g Na_2S and 1.58 g Na_2SO_3; 10 mg of catalyst	300 W xenon lamp	1718	9
CdS/np-rGO	Na_2S/Na_2SO_3 mixture with concentration of 0.25 M/0.35 M; 10 mg of catalyst	300 W xenon lamp (420 nm <λ< 760 nm)	2171.23	10
CdS quantum dots/In_2O_3	5 mL of deionized water and 1 mL of TEOA; 5 mg of catalyst	300 W xenon lamp with a filter (λ > 420 nm)	2258.59	11
Al-MOF/0.3CZS	20 vol% of lactic acid; 30 mg of catalyst	300 W xenon lamp (350 nm <λ< 780 nm)	4007	This work

Table S5 The fitting parameters of the TR-PL spectra of Al-MOF and Al-MOF/x-CZS.

Samples	A1	A2	A3	τ_1(ns)	τ_2(ns)	τ_3(ns)	R^2	τ_{ave}(ns)
Al-MOF	0.696	0.245	0.103	0.622	2.748	7.777	0.996	4.378
Al-MOF/0.15CZS	0.747	0.305	0.084	0.762	0.762	6.004	0.990	2.786
Al-MOF/0.3CZS	0.578	0.321	0.121	0.567	0.567	4.189	0.997	2.373
Al-MOF/0.5CZS	0.575	0.403	0.055	0.621	0.621	4.758	0.995	1.867

Table S6 Parameters of the equivalent circuit for the impedance data of Al-MOF, CZS and Al-MOF/x-CZS.

Samples	Rs (Ω)	Rp (Ω)
CZS	4.59	28.97
Al-MOF	4.24	59.45
Al-MOF/0.15CZS	3.80	47.57
Al-MOF/0.3CZS	4.61	33.49
Al-MOF/0.5CZS	4.37	44.86

References

1. Z. Dong, D. Li, T. Han, X. Zhao and X. Lei, Boosting solar hydrogen generation by growth of UiO-based MOF on metal sulfide surface, *J. Environ. Chem. Eng.*, 2025, **13**, 116141.
2. X. Li and Z. Jin, Rational Construction of 2D/3D Co_3O_4/NH_2 - MIL - 53(Al) Heterostructures to Facilitate Photocatalytic Hydrogen Evolution, *Solar RRL*, 2023, **7**, 2300160.
3. B. Zhao, J. Liu, Y. Liu, W. Wen and Z. Li, In situ growth of ZnCdS nanoparticles on bimetallic Cu/Fe-MOF for efficient visible-light-driven photocatalytic hydrogen production and urea synthesis, *J. Alloys Compd.*, 2025, **1011**, 178395.
4. W. Li, J. Li, H. Ma, R. Xiong, P. Fang, C. Pan and J. Wei, Efficient spatial separation of charge carriers over Sv-$ZnIn_2S_4/NH_2$-MIL-88B(Fe) S-scheme heterojunctions for enhanced photocatalytic H2 evolution and antibiotics removal performance, *J. Colloid Interface Sci.*, 2024, **657**, 728-737.
5. H. Chen, J. Wu, Y. Zhu, J. Yang, B. Tang, T. Zhang and H. Yang, Cu-MOF modified $ZnIn_2S_4$ nanosheet composite catalyst for photocatalytic hydrogen production, *Renewable Energy*, 2024, **228**, 120672.
6. Z. Liu, J. Xu, T. Xue, X. Liu, S. Xu and Z. Li, Hydrogen evolution performance of Co-MOF/H-g-C_3N_4 composite catalysts with different morphologies under visible light, *New J. Chem.*, 2023, **47**, 3703-3713.
7. X. Sun, Z. Yi, S. Wang, G. Liu, X. Wang and H. Yang, Interface electric field and photothermal effect of Ag_2S@CdZnS hollow heterostructures synergistically boosting photocatalytic H_2 evolution, *Sep. Purif. Technol.*, 2026, **385**, 136365.
8. R. Qi, X. Sun, S. Wang, Z. Yi, G. Liu and H. Yang, Boosting photocatalysis of metal sulfides for H_2 evolution through Hads–S antibonding-orbital regulation by Ag medium, *Mater. Today Energy*, 2025, **54**, 102142.

9. X. Gui, Y. Zhou, Q. Liang, M. Zhou, X. Li, S. Xu and Z. Li, Construction of porous ZnS/TiO_2 S-scheme heterostructure derived from MOF-on-MOF with boosting photocatalytic H_2-generation activity, *Int. J. Hydrogen Energy*, 2023, **48**, 38237-38250.
10. C. Yuan, H. Lv, Y. Zhang, Q. Fei, D. Xiao, H. Yin, Z. Lu and Y. Zhang, Three-dimensional nanoporous heterojunction of CdS/np-rGO for highly efficient photocatalytic hydrogen evolution under visible light, *Carbon*, 2023, **206**, 237-245.
11. Y.-H. Wu, Y.-Q. Yan, Y.-X. Deng, W.-Y. Huang, K. Yang and K.-Q. Lu, Rational construction of S-scheme CdS quantum dots/In_2O_3 hollow nanotubes heterojunction for enhanced photocatalytic H2 evolution, *Chinese Journal of Catalysis*, 2025, **70**, 333-340.